Original Research Article: full paper

(2023), «EUREKA: Physics and Engineering»
Number 3

INVESTIGATION ON HIGH-STRENGTH LOW ALLOY 0.35Cr-1.9Ni-0.55Mo STEEL DEPOSITED ON 20Cr SUBSTRATE BY WIRE AND ARC-BASED DIRECTED ENERGY DEPOSITION

Duong Vu
School of Engineering Technology
Duy Tan University
03 Quang Trung str., Da Nang, Vietnam, 550000

Van Thao Le ✉
Advanced Technology Center (ATC)
Le Quy Don Technical University
236 Hoang Quoc Viet str., Bac Tu Liem Dist., Hanoi, Vietnam, 10000
thaomta@gmail.com

✉**Corresponding author**

Abstract

This article aims to observe the microstructure, mechanical properties, and interface bonding of a 0.35Cr-1.9Ni-0.55Mo alloy deposited on 20Cr steel by wire and arc-based directed energy deposition (WA-DED). For this purpose, different characterization techniques such as an optical microscope, scanning electron microscopy (SEM) with energy dispersive spectroscopy (EDS), and a high-resolution X-ray diffractometer were used to analyze the microstructure, chemical composition, and phases of the deposited material. Microhardness and tensile tests were also carried out. The results show that the microstructure of the deposited material is relatively homogeneous, with a slight increase in grain size from the bottom to the top of the deposited part, thus resulting in a slightly decreasing trend in microhardness. However, the ranges of hardness values, i.e., 288 ± 16.78 HV0.1 (in the bottom) to 256 ± 17.04 HV0.1 (in the top), overlap very significantly, and they are not statistically different. The heat-affected zone (HAZ) is the hardest (301 ± 2.70 HV0.1), while the substrate has the lowest microhardness (203 ± 17.64 HV0.1). The tensile strengths of deposited materials are relatively isotropic in both the horizontal (HD) and vertical (VD) directions: UTS_{VD} = 1013 ± 9.29 MPa, UST_{HD} = 985 ± 24.58 MPa, $YS_{(0.2\,\%)VD}$ = 570 ± 4.51 MPa, and $YS_{(0.2\,\%)HD}$ = 614 ± 19.66 MPa. The tensile strengths of interface specimens are also comparable to those of the substrate materials (e.g., 951 vs. 972 MPa in UTS), indicating excellent metallurgical bonding between the deposited and substrate materials. The results of this work confirm the efficiency of the WA-DED technique to produce high-quality components in industry.

Keywords: WA-DED, microstructure, mechanical properties, phase transformation, interface bonding.

DOI: 10.21303/2461-4262.2023.002837

1. Introduction

Directed Energy Deposition (DED) refers to a category of additive manufacturing or 3D printing techniques involving a coaxial powder or wire feed to an energy source. (DED) is a category of metal additive manufacturing (AM) technologies that are widely investigated to produce large-size components in the marine, aeronautic, and mold and die industries. The DED technologies can be classified into powder-feeding and wire-feeding DED processes. In the wire-feeding DED process, an electric arc is applied to melt the metal wire. Wire and arc-based directed energy deposition (WA-DED) is a metal additive manufacturing technology that enables the production of large-size components due to its wide and flexible building space and high rate of metal deposition [1].

In the literature, many steel grades have been investigated and fabricated with the WA-DED processes, e.g., low-carbon steels, austenite stainless steels, and high-strength low-alloy (HSLA) steels [2–4]. In comparison with carbon steel, HSLA provides better mechanical properties, especially corrosion resistance. They have good weldability. The alloy elements such as chromium, nickel, and molybdenum tend to modify the microstructure of the carbon steel to produce a very fine dispersion of alloy carbides in a ferrite matrix. This improves the toughness of the materials. The 0.35Cr-1.9Ni-0.55Mo alloy is a HSLA steel that is widely used to manufacture parts in the automotive, shipbuilding, and tooling industries. This steel has high strength, weldability, and low costs [5].

Recently, several studies have reported on the WA-DED process of HSLA steels. For example, the HSLA steel walls were built by WA-DED, and the anisotropy in mechanical characteristics has been observed [6]. In the WA-DED process, the heat input has an important role to the microstructures and mechanical properties of HSLA steel part [7]. The toughness properties of HSLA steels produced by WA-DED were also investigated in [8]. However, most of the published studies only focused on the metallurgical characterization of the deposited material. Practically, in many cases, parts fabricated by WA-DED can also include the substrate material. The deposited and substrate materials will work together. Both the deposited and substrate materials, as well as the interface bonding between them, must be analyzed. Therefore, this study aims to fill this research gap and confirm the internal quality of WA-DED parts for industrial applications.

2. Materials and methods

In this paper, a wire and arc-based directed energy deposition (WA-DED) system, including a gas metal arc welding source with a welding torch, a 6-axis robot, a wire feed system, and a shielding gas system, was adopted to fabricate the samples (**Fig. 1**).

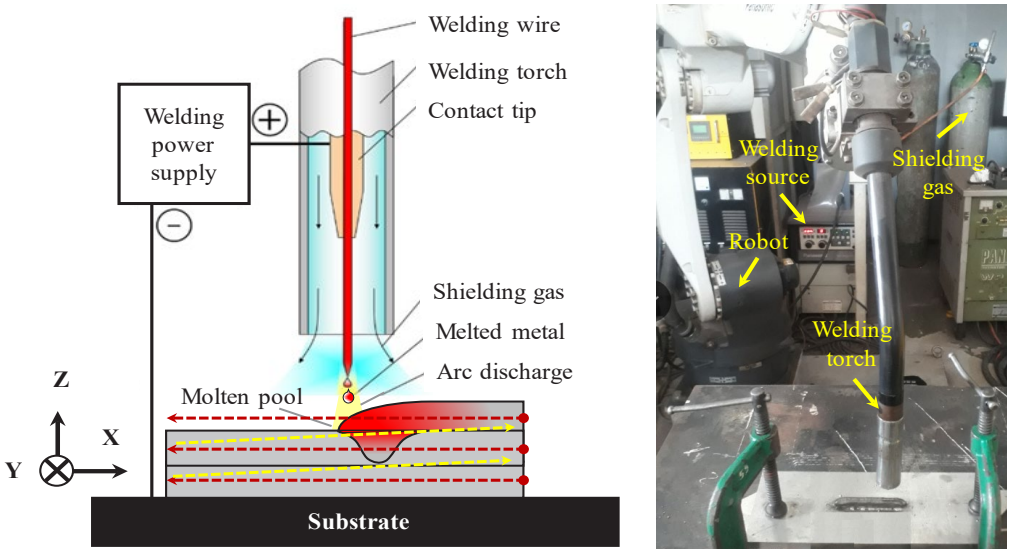

a *b*

Fig. 1. The WA-DED process: *a* – the schema; *b* – the real system

The microstructures were observed by an optical microscope (A2M AXIO imager, Carl Zeiss). The chemical composition and microstructures were analyzed with the EDS technique integrated in a scanning electron microscope (SEM, model SU3500). The phase analysis of the deposited and substrate materials was performed on a high-resolution X-ray diffractometer (ARL Equinox 5000 Series). The X-ray computed tomography (CT) technique was employed to assess the porosity. The microhardness was also tested by a hardness tester (Duramin-2, Struers). Each test was performed with a load of 980.70 mN and a dwell time of 10 s. All the tensile specimens were designed according to the ASTM E8M-13 standard. The tensile tests were carried out on a tensile machine. The tensile velocity was 12 mm per minute. The broken surfaces of the samples were observed by the SEM technique. The 0.35Cr-1.9Ni-0.55Mo alloyed steel wire with 1.2 mm in diameter was used as the feedstock material, and the 20Cr steel cylinder with 100 mm in diameter and 80 mm in height was used as the substrate to fabricate the double-bead multilayer sample, which was intended for the characterization of microstructures and mechanical properties in the vertical direction (VD) (**Fig. 1, *a*, *b***). Another double-bead multilayer sample was fabricated from the same welding wire to analyze the tensile properties of the deposited material in the horizontal direction (HD) (**Fig. 1**). The chemical composition of the wire [9] includes 0.089 % C, 0.80 % Si, 1.90 % Mn, 0.010 % P, 0.004 % S, 1.95 % Ni, 0.34 % Cr, 0.58 % Mo, and bal. % Fe in wt. %, while the composition of the substrate

material (20Cr steel) is (0.18–0.24) % C, (0.17–0.37) % Si, (0.50–0.80) % Mn, (0.70–1.00) % Cr, (≤0.03) % P/S/Cu/Ni/Mo, and bal. % Fe in wt. %. According to [10], the 20Cr steel has the following mechanical properties:

– tensile strength: ≥835 N/mm^2;
– yield strength: ≥540 N/mm^2;
– elongation after break: ≥10 %;
– rate of reduction in area: ≥40 %;
– impact absorbing energy: ≥47 J;
– material Brinell hardness: ≤179 (annealing or high temperature tempering state);
– test sample size: 15 mm.

The deposition strategy of the samples was illustrated in **Fig. 1, *a***. Each layer is composed of two weld tracks with an overlap of 0.65 weld track width. The narrows show the weld track direction. The length of a weld track is 80 mm. The process parameters used to fabricate the samples include 120 A in current, 20 V in voltage, and 0.3 m/min in travel speed. The shielding gas of 80 % Ar and 20 % CO_2 with 16 L/min in flow speed was used during the deposition. The dwell time between two successive layers was 40 s.

To prepare the microstructure specimen and the vertical tensile specimens, the first deposited sample (**Fig. 2, *b***) was cut through the planes (*P*) and (*Q*) to remove the side surface of the deposited wall and to obtain the core of the deposited and substrate materials; subsequently, the vertical tensile specimens were extracted in the three regions, i.e., the deposited zone (VD-1,2,3), interface zone (IR-1,2,3), and substrate zone (S-1,2,3), and the MS specimen was extracted to analyze the microstructure, phase transformation, and microhardness, as illustrated in **Fig. 2, *a***. The horizontal tensile specimens were extracted from the second deposited sample (**Fig. 2, *c***). The dimensions of the tensile specimens are shown in **Fig. 2, *e***. The schema of microstructure specimens shown in **Fig. 2, *d***.

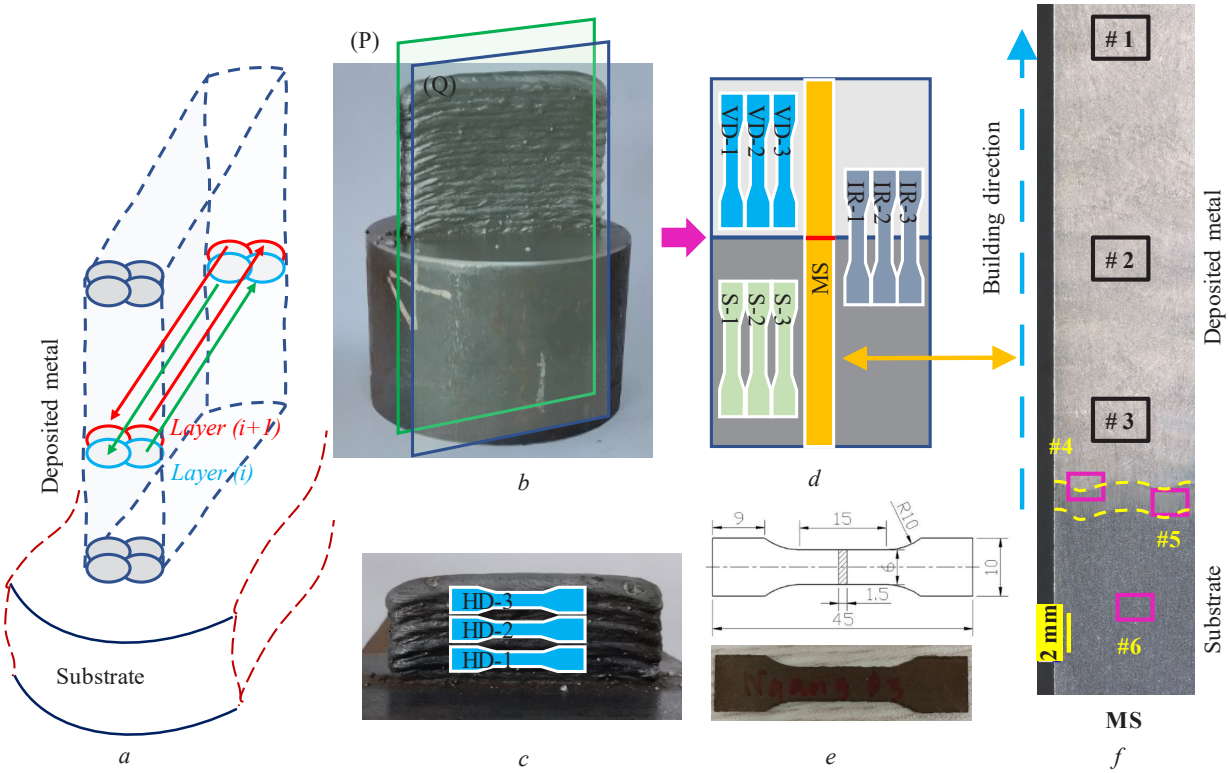

Fig. 2. Fabrication of samples: *a* – the deposition strategy; *b* – deposited sample for analyzing microstructures, microhardness, and vertical tensile properties; *c* – deposited sample for analyzing horizontal tensile properties; *d* – schema of microstructure specimens (MS) and vertical tensile specimens; *e* – an extracted tensile specimen and its design dimensions; *f* – locations for observing microstructures and microhardness on MS

Before observing the microstructure, the MS specimen was ground, polished, and chemically etched. The microstructures of the deposited and substrate materials were analyzed using a digital optical microscope (OM) and a scanning electron microscope (SEM) on the specimen MS in different regions, including #1, #2, and #3, corresponding to the top, middle, and bottom of the deposited part; #4, the interface region between the deposited and substrate materials; #5, the heat-affected zone (HAZ); and #6, the substrate region. The phase in microstructure was analyzed using X-ray diffraction (XRD). The microhardness was measured by a microhardness machine. Each test was performed with a load of 980.7 mN and 10 s of dwell time. The tensile tests were carried out on a tensile tester at room temperature with a crosshead speed of 10 mm/min.

3. Results and discussion

3. 1. Microstructures

Fig. 3 shows the OM images of microstructures of both the deposited and substrate materials in different regions. It is revealed that the as-fabricated part is fully dense. There are no major defects, such as lack of fusion, pores, or cracks inside the deposited part or between the deposited material and the substrate. In fact, during the WA-DED process, as the material is deposited layer-by-layer, the temperature of the earlier layers rises, slowing down the cooling process and reducing the susceptibility to cold cracking. Furthermore, the absence of mechanical constraints in WA-DED, which happens during welding, enables the material to tolerate some thermal stresses created during the deposition, which further lowers the likelihood of cold cracking.

In terms of microstructure, all three regions of the deposited material, i.e., the top (#1, #1b), middle (#2, #2b), and bottom (#3, #3b), reveal the same microstructure of the ferrite phase with dominant acicular and little granular morphologies. This observation is confirmed by the XRD analysis results (**Fig. 4**). In all three regions (the top #1, middle #2, and bottom #3), the deposited metal features totally ferrite phases with three peaks: (110), (200), and (211). There are no peaks corresponding to oxide phases that were detected in the XRD patterns. This can be explained by the low percentage of alloying elements in the deposited metal (welding wire).

For high-strength low-alloy (HSLA) steels, the solid-state transformation occurs as follows: when the temperature decreases from 1300 to 800 °C, the austenitic grains are nucleated and developed from the liquid phase. After that, when the temperature is cooled down from 800 to 500 °C, austenite phases are transformed into bainite and different ferrite phases [11]. Allotriomorphic ferrite is formed at the boundaries of prior austenite grains, and then side-plate ferrite may be nucleated at the boundaries of austenite and ferrite. The formation of acicular ferrite is generally related to oxide inclusions and cooling conditions. Depending on the carbon content, the remaining austenite may be partially or completely transformed into martensite during the final cooling period to room temperature [7, 12]. However, in the current study, martensite phases were not observed in the as-deposited material. This is because the cooling rate did not exceed 100 °C/s during the WA-DED process of the studied alloy [7].

Moreover, it is found that the bottom region shows the finest microstructure, followed by the middle and top regions, respectively. The average grain size is about 0.72 ± 0.17 μm in the bottom (**Fig. 3, *c*, *i***), 0.87 ± 0.18 μm in the middle (**Fig. 3, *b*, *h***), and 1.21 ± 0.40 μm in the top (**Fig. 3, *a, g***). This phenomenon is related to the decrease in cooling rate as the number of deposited layers increases. In the WA-DED process, as the deposited layers increase, the previous layers' temperature increases (also known as the heat accumulation phenomenon in DED processes). As a result, the grains are coarser along the building direction.

Fig. 3, *d* shows the microstructure in the interface zone between the deposited material and the substrate. There were no defects, such as cracks or a lack of fusion, in the interface zone. The microstructure of the substrate (**Fig. 3, *f***) is composed of polygonal ferrite and pearlite [13]. However, under the effect of the heat source that formed the first deposited layer, the polygonal grains in the substrate zone were transformed into the fine grains in the HAZ (**Fig. 3, *e***). No defects exist, and the continuous transition of microstructure in the interface zone confirms a good bonding in terms of metallurgy between the deposited and substrate materials. The phases observed in the OM analysis were also confirmed by the XRD results (**Fig. 4**).

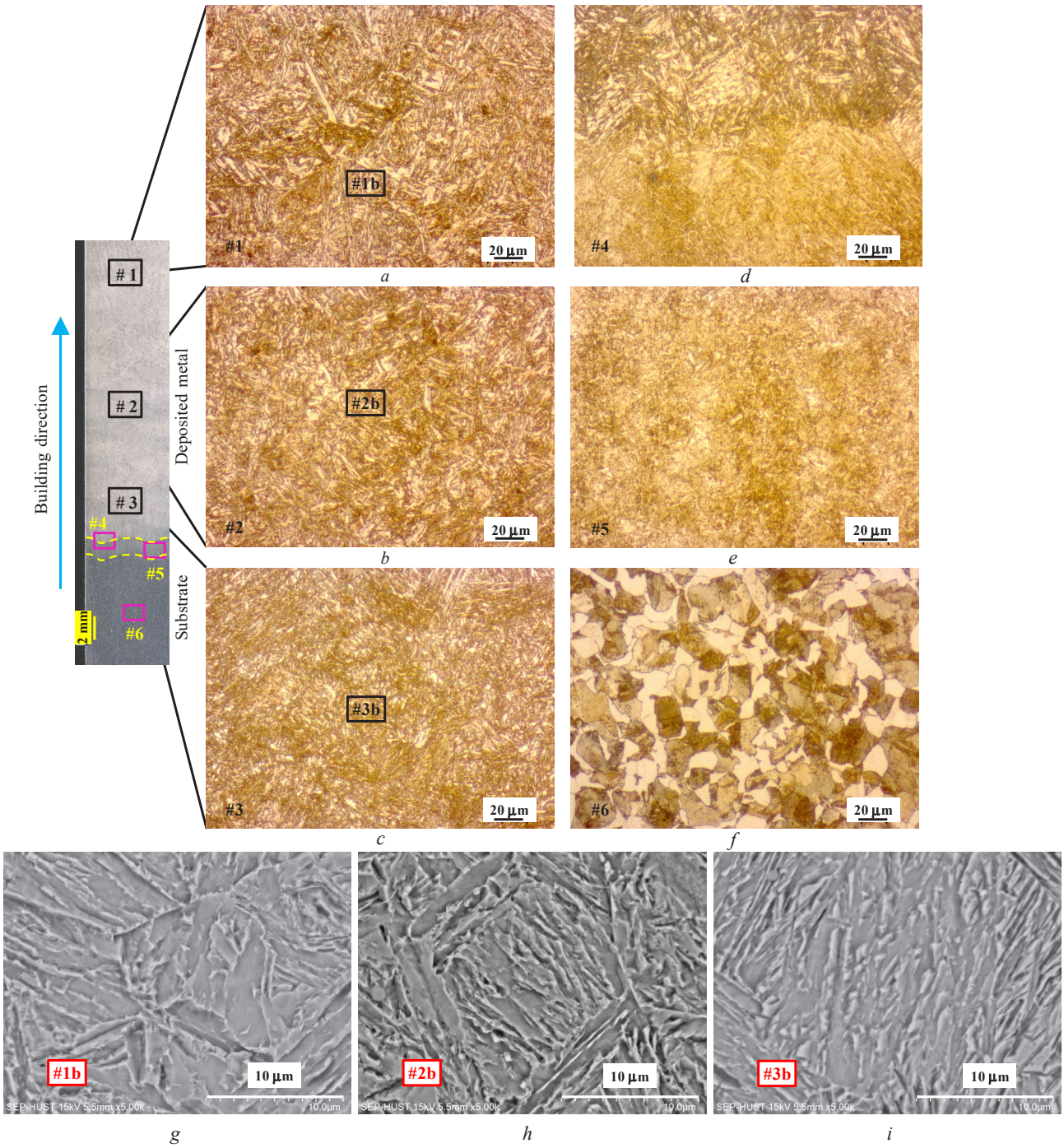

Fig. 3. OM images of microstructures in different zones:
a – top, *b* – middle, *c* – bottom of the deposited metal, *d* – the interface between the deposited metal and the substrate, *e* – HAZ, and *f* – the substrate zone; *g*–*i* – the SEM images from #1b, #2b, and #3b zones, respectively

According to the SEM-EDS analysis results (**Fig. 5**), it is revealed that the percentage in weight of chemical elements (e.g., Cr, Ni, Mn, Mo, and Si) in different deposited layers is nearly homogenous. It is worth noting that the EDS technique is limited to detecting elements with a weight percentage inferior to 0.1 % [14].

Therefore, the chemical components such as C, P, S, and Cu were not included in the analysis of the weight percentage.

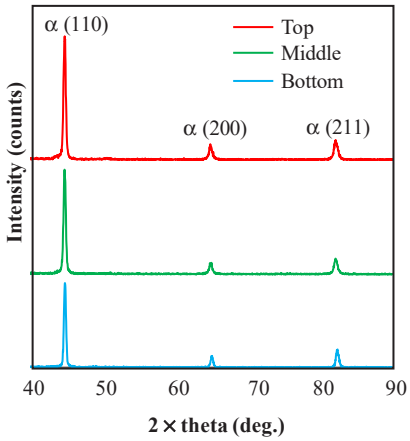

Fig. 4. Results of XDR analysis

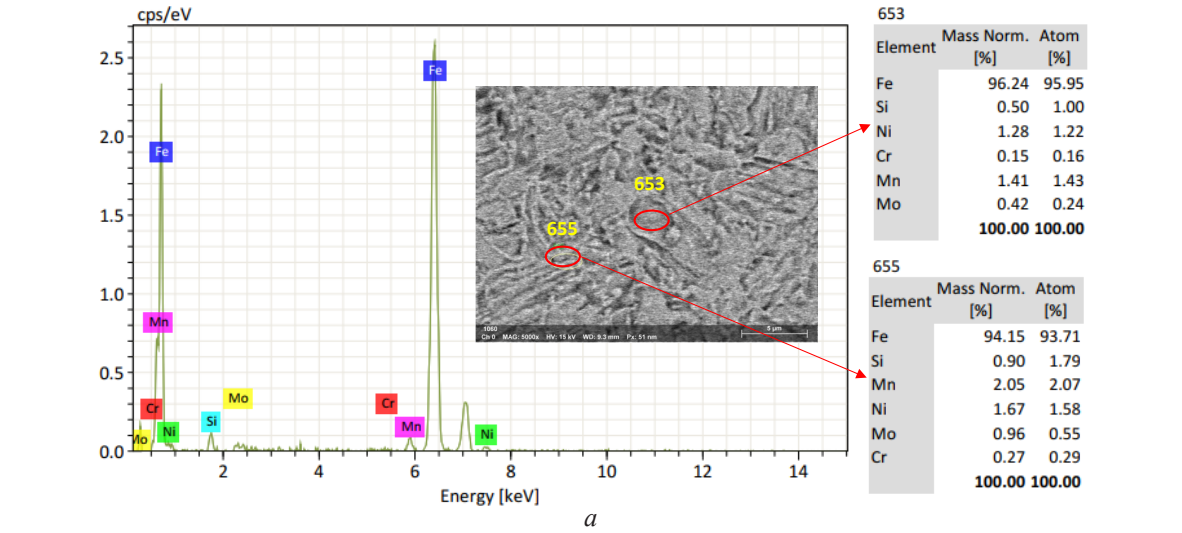

a

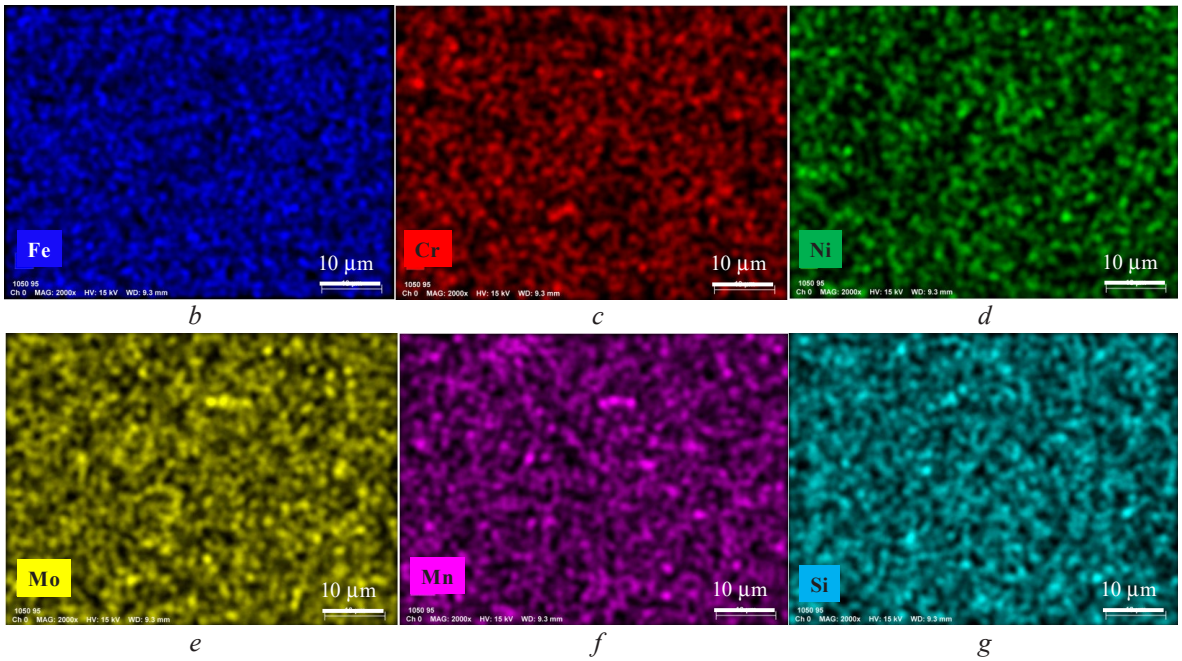

b *c* *d*

e *f* *g*

Fig. 5. Analysis EDX for the deposited material: *a* – chemical composition result, *b*–*g* – the mapping of elements Fe, Cr, Ni, Mo, Mn, and Si, respectively

3. 2. Mechanical properties

Fig. 6 shows all the curves of stress and strain for all tested tensile specimens. All specimens begin with the elastic deformation in the initial step, and the following step is the plastic deformation before the fractured.

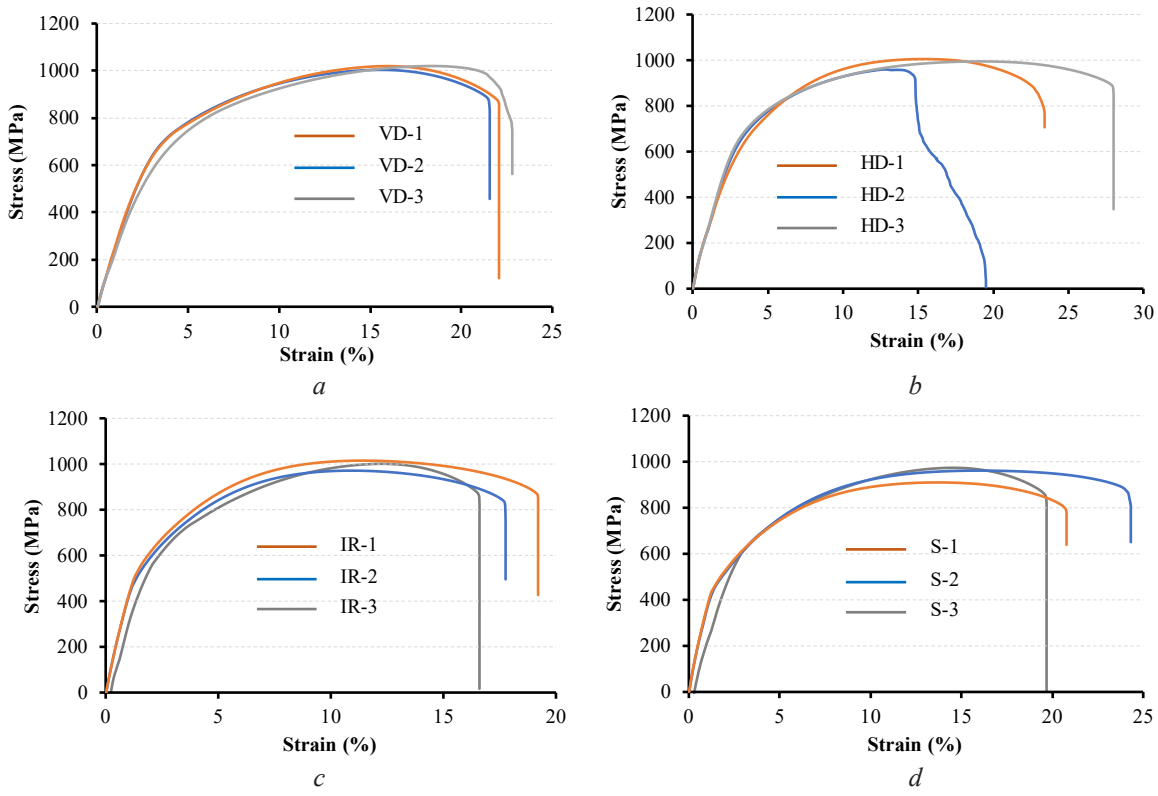

Fig. 6. Stress-strain curves for the tensile specimens:
a – VD, *b* – HD, *c* – IF, *d* – S

Fig. 7, *a*, *b* display the hardness distribution in different regions of deposited and substrate materials. It is revealed that the HAZ (#5) shows the highest hardness (301 ± 22.70 HV0.1). The substrate reveals the lowest hardness (203 ± 17.64 HV0.1). In the deposited part, the hardness shows a slightly decreasing tendency along the building direction. The results of the hardness analysis are in good agreement with the microstructure previously observed. According to the Hall-Petch behavior [15, 16], the hardness decreases with an increase in grain size. In the deposited part, due to the reheating cycles and heat accumulation, the grains are coarse along the build direction and along the layer height, as discussed previously. Hence, the average microhardness gradually decreases along the depositing direction. The high-cooling rate occurred at the bottom because it was directly deposited on the cold plate, resulting in the smallest grains in microstructures. Therefore, the highest average hardness was achieved. However, the ranges of hardness values of the deposited material – i.e., 288 ± 16.78 HV0.1 (in the bottom) to 256 ± 17.04 HV0.1 (in the top), overlap very significantly, and they are not statistically different.

Fig. 7, *c* shows a comparison of tensile properties between different directions and regions. It is shown that the tensile properties (YS – yield strength; UTS – ultimate tensile strength, EL – elongation) of the deposited layer in the vertical (VD) and horizontal (HD) directions are comparable with a slight difference: $UTS_{VD} = 1013 \pm 9.29$ MPa, $UTS_{HD} = 985 \pm 24.58$ MPa, $YS_{(0.2\,\%)VD} = 570 \pm 4.51$ MPa, $YS_{(0.2\,\%)HD} = 614 \pm 19.66$ MPa, $EL_{VD} = 22 \pm 0.58$ %, $EL_{HD} = 23 \pm 0.4.51$ %. This indicates a relative isotropy in the tensile properties of the deposited material. The interface tensile specimens (IR) also feature relatively comparable values versus those of the substrate tensile specimen (S): $UTS_{IR} = 951 \pm 34.43$ MPa, $UTS_S = 972 \pm 25.12$ MPa, $YS_{(0.2\,\%)IR} = 493 \pm 19.55$ MPa,

$YS_{(0.2\,\%)S} = 514 \pm 12.16$ MPa, $EL_{IR} = 25 \pm 4.58$ %, and $EL_S = 18 \pm 1.53$ %. Moreover, all the IR specimens were broken in the substrate metal instead of at the interface. This confirmed that the substrate and the deposited part were strongly bonded and that the deposition process was reliable and stable.

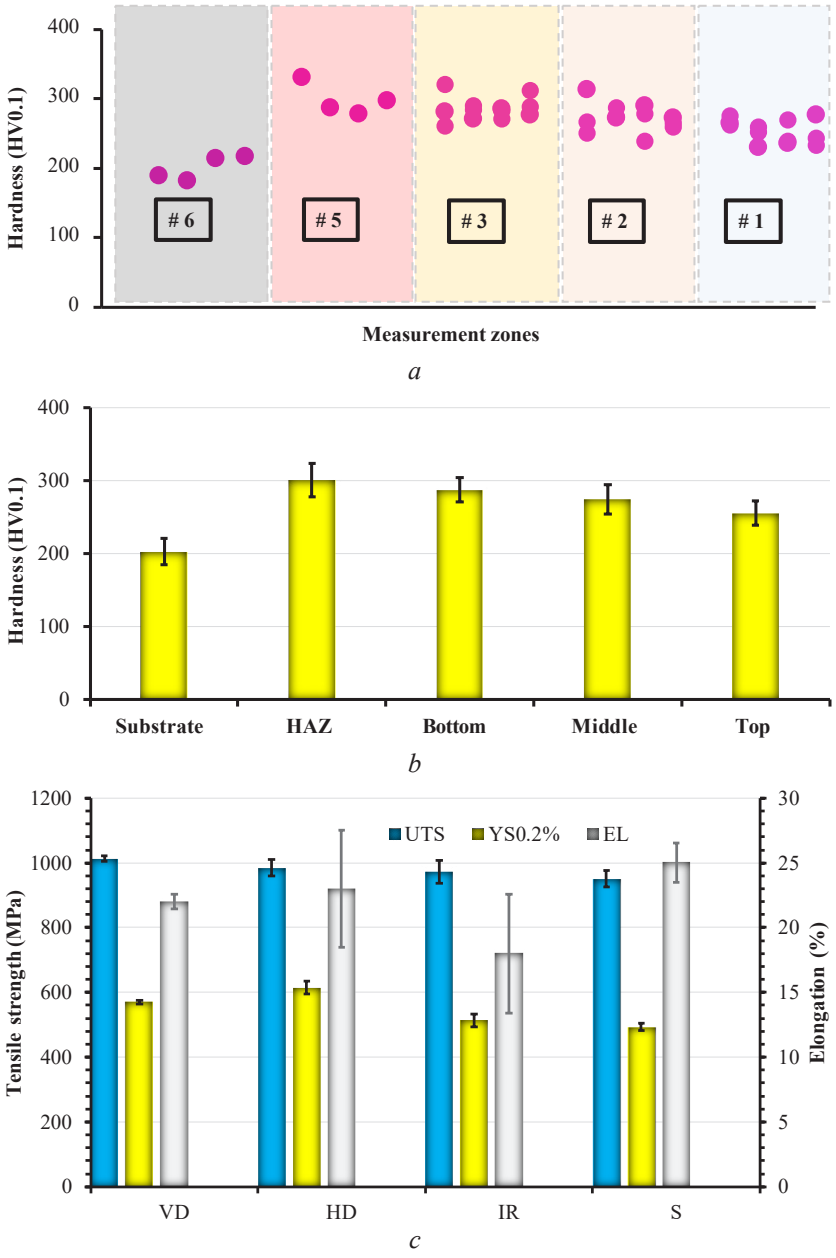

Fig. 7. Mechanical properties: *a* – hardness distribution, *b* – average hardness value in different zones, and *c* – comparison of tensile properties between different specimens

3. 3. Limitations of the study and development prospect

Based on the obtained results, it can be found that the strength of the deposited materials can be comparable to those of the wrought ones (e.g., the UTS of the wire is ≥760 MPa), confirming that the deposited material can satisfy real working conditions. However, herein, the material strength was only tested on a simple sample. In some circumstances, the proper selection of the material is also an issue. For real applications, components will have more complex geometry, which requires more complex deposition paths during the fabrication process, and the fabricated components will introduce more residual stress and thermal deformation. In these cases, heat treatment

post-processing will be required to obtain the expected properties and reduce residual stress. Moreover, fabricated components should be tested under real loading conditions. Hence, in future works, the fabrication of parts and components for specific applications will be focused. Moreover, the post-processing of as-deposited components, such as heat treatment and machining of functional surfaces, will be investigated, taking into account the production cost and productivity.

4. Conclusions

In this paper, the microstructure, mechanical properties, and interface bonding of the 0.35Cr-1.9Ni-0.55Mo alloy deposited on 20Cr steel by the WA-DED process were investigated. The main findings are as follows.

The deposited material features total ferrite phases with acicular and granular morphologies, whereas the hot-rolled substrate shows equiaxial grains of ferrite and perlite. The microstructure of the deposited material is relatively homogenous with a slight increase in grain size along the build direction.

There is a continuous transformation in microstructure without a lack of fusion between the deposited and substrate materials. The microstructure of the substrate in HAZ is refined under the effect of the heat source of the deposition process.

The hardness in the deposited part shows a slightly decreasing trend. However, the ranges of hardness value – i.e., 288 ± 16.78 HV0.1 (in the bottom) to 256 ± 17.04 HV0.1 (in the top), overlap very significantly, and they are not statistically different. Meanwhile, the HAZ is the hardest (301 ± 22.70 HV0.1), and the substrate features the lowest hardness (203 ± 17.64HV).

The tensile strengths of deposited materials are relatively isotropic in both the horizontal and vertical directions. The tensile strengths of interface specimens are also comparable to those of the substrate (e.g., 972 vs. 951 MPa in UTS), indicating excellent bonding between the deposited and substrate materials.

Conflict of interest

The author declares that they have no conflict of interest in relation to this research, whether financial, personal, authorship or otherwise, that could affect the research and its results presented in this paper.

Financing

The study was performed without financial support.

Data availability

Data will be made available on reasonable request.

References

[1] Williams, S. W., Martina, F., Addison, A. C., Ding, J., Pardal, G., Colegrove, P. (2016). Wire + Arc Additive Manufacturing. Materials Science and Technology, 32 (7), 641–647. doi: https://doi.org/10.1179/1743284715y.0000000073

[2] Wu, B., Pan, Z., Ding, D., Cuiuri, D., Li, H., Xu, J., Norrish, J. (2018). A review of the wire arc additive manufacturing of metals: properties, defects and quality improvement. Journal of Manufacturing Processes, 35, 127–139. doi: https://doi.org/10.1016/j.jmapro.2018.08.001

[3] Jin, W., Zhang, C., Jin, S., Tian, Y., Wellmann, D., Liu, W. (2020). Wire Arc Additive Manufacturing of Stainless Steels: A Review. Applied Sciences, 10 (5), 1563. doi: https://doi.org/10.3390/app10051563

[4] Le, V. T., Mai, D. S., Doan, T. K., Paris, H. (2021). Wire and arc additive manufacturing of 308L stainless steel components: Optimization of processing parameters and material properties. Engineering Science and Technology, an International Journal, 24 (4), 1015–1026. doi: https://doi.org/10.1016/j.jestch.2021.01.009

[5] Cochrane, R. C. (2012). Phase transformations in microalloyed high strength low alloy (HSLA) steels. Phase Transformations in Steels, 153–212. doi: https://doi.org/10.1533/9780857096111.2.153

[6] Sun, L., Jiang, F., Huang, R., Yuan, D., Guo, C., Wang, J. (2020). Anisotropic mechanical properties and deformation behavior of low-carbon high-strength steel component fabricated by wire and arc additive manufacturing. Materials Science and Engineering: A, 787, 139514. doi: https://doi.org/10.1016/j.msea.2020.139514

[7] Rodrigues, T. A., Duarte, V., Avila, J. A., Santos, T. G., Miranda, R. M., Oliveira, J. P. (2019). Wire and arc additive manufacturing of HSLA steel: Effect of thermal cycles on microstructure and mechanical properties. Additive Manufacturing, 27, 440–450. doi: https://doi.org/10.1016/j.addma.2019.03.029

[8] Dirisu, P., Ganguly, S., Mehmanparast, A., Martina, F., Williams, S. (2019). Analysis of fracture toughness properties of wire + arc additive manufactured high strength low alloy structural steel components. Materials Science and Engineering: A, 765, 138285. doi: https://doi.org/10.1016/j.msea.2019.138285

[9] SM-110, AWS A5.28/ASME SFA-5.28 ER110S-G (2002). Huyndai Welding, Rev 0.3.

[10] Grade 20Cr Steel Composition, Properties, Material Equivalent. World Material. Available at: https://www.theworldmaterial.com/20cr-steel/

[11] Shi, Y., Han, Z. (2008). Effect of weld thermal cycle on microstructure and fracture toughness of simulated heat-affected zone for a 800MPa grade high strength low alloy steel. Journal of Materials Processing Technology, 207 (1-3), 30–39. doi: https://doi.org/10.1016/j.jmatprotec.2007.12.049

[12] Duarte, V. R., Rodrigues, T. A., Schell, N., Santos, T. G., Oliveira, J. P., Miranda, R. M. (2021). Wire and Arc Additive Manufacturing of High-Strength Low-Alloy Steel: Microstructure and Mechanical Properties. Advanced Engineering Materials, 23 (11), 2001036. doi: https://doi.org/10.1002/adem.202001036

[13] Liu, H., Dong, Y., Zheng, H., Liu, X., Lan, P., Tang, H., Zhang, J. (2021). Precipitation Criterion for Inhibiting Austenite Grain Coarsening during Carburization of Al-Containing 20Cr Gear Steels. Metals, 11 (3), 504. doi: https://doi.org/10.3390/met11030504

[14] Willis, R. D., Blanchard, F. T., Conner, T. L. (2002). Guidelines for the Application of SEM/EDX Analytical Techniques to Particulate Matter Samples. Technical Report.

[15] Singh, K. K., Sangal, S., Murty, G. S. (2002). Hall-Petch behaviour of 316L austenitic stainless steel at room temperature. Materials Science and Technology, 18 (2), 165–172. doi: https://doi.org/10.1179/026708301125000384

[16] Zhang, H., Liu, F., Ungar, G., Zheng, Z., Sun, Q., Han, Y. (2022). A regime beyond the Hall-Petch and inverse-Hall-Petch regimes in ultrafine-grained solids. Communications Physics, 5 (1). doi: https://doi.org/10.1038/s42005-022-01107-7

Received date 24.01.2023
Accepted date 21.03.2023
Published date 25.05.2023

How to cite: *Vu, D., Le, V. T. (2023). Investigation on high-strength low alloy 0.35Cr-1.9Ni-0.55Mo steel deposited on 20Cr substrate by wire and arc-based directed energy deposition. EUREKA: Physics and Engineering, 3, 166–175. doi: https://doi.org/10.21303/2461-4262.2023.002837*